

Enhancement of electromagnetically induced absorption and four-wave mixing in a double two-level system

Yu-Sen Wang(王禹森) and Ying-Jie Du(杜英杰)

Citation: Chin. Phys. B, 2025, 34 (**12**): 124201. DOI: 10.1088/1674-1056/ade8e1
http://cpb.iphy.ac.cn; http://iopscience.iop.org/cpb

What follows is a list of articles you may be interested in

Enhancement of four-wave mixing due to coherent hole burning in a degenerate two-level system

Zhi-Yuan Liu(刘知远), Yi-Fan Yao(姚一凡), Yue Sun(孙悦), Jia-Yu Han(韩佳瑜), and Ying-Jie Du(杜英杰)
Chin. Phys. B, 2025, 34 (**5**): 054203. DOI: 10.1088/1674-1056/adb949

Electromagnetically-induced-absorption-like ground state cooling in a hybrid optomechanical system

Yaoyong Dong(董耀勇), Xuejun Zheng(郑学军), Denglong Wang(王登龙), and Peng Zhao(赵鹏)
Chin. Phys. B, 2025, 34 (**4**): 044203. DOI: 10.1088/1674-1056/adb260

Intrinsic polarization conversion and avoided-mode crossing in X-cut lithium niobate microrings

Zelin Tan(谭泽林), Jianfa Zhang(张检发), Zhihong Zhu(朱志宏), Wei Chen(陈伟), Zhengzheng Shao(邵铮铮), Ken Liu(刘肯), and Shiqiao Qin(秦石乔)
Chin. Phys. B, 2024, 33 (**6**): 064205. DOI: 10.1088/1674-1056/ad47b2

Electromagnetically induced transparency and electromagnetically induced absorption in Y-type system

Kalan Mal, Khairul Islam, Suman Mondal, Dipankar Bhattacharyya, Amitava Bandyopadhyay
Chin. Phys. B, 2020, 29 (**5**): 054211. DOI: 10.1088/1674-1056/ab7ea0

Controllable optical response in hybrid opto-electromechanical systems

Jiang Cheng (江成), Cui Yuan-Shun (崔元顺), Liu Hong-Xiang (刘洪香), Li Xiao-Wei (李晓薇), Chen Gui-Bin (陈贵宾)
Chin. Phys. B, 2015, 24 (**5**): 054206. DOI: 10.1088/1674-1056/24/5/054206

Enhancement of electromagnetically induced absorption and four-wave mixing in a double two-level system

Yu-Sen Wang(王禹森)[1] and Ying-Jie Du(杜英杰)[1,2,†]

[1] *School of Physics, Northwest University, Xi'an* 710127, *China*

[2] *Collaborative Innovation Center of Extreme Optics, Shanxi University, Taiyuan* 030006, *China*

(Received 18 April 2025; revised manuscript received 11 June 2025; accepted manuscript online 27 June 2025)

We present a theoretical investigation of the electromagnetically induced absorption (EIA) due to transfer of population (TOP) in the double two-level system (TLS). It shows that one TLS is responsible for the sub-natural absorption part of EIA, and the other TLS is responsible for the natural absorption part of EIA. We propose a scheme in which the sub-natural absorption part of EIA is governed by the effect of coherent hole burning (CHB) and achieves an enhancement of at least two orders of magnitude with the detuned coupling field, while the natural absorption part is dominated by the effect of Mollow absorption (MA) and does not change with the detuned coupling field. Due to the effects of CHB and MA, the magnitude of four-wave mixing (FWM) achieves a significant increase for double TLS. We show in detail the evolution of the magnitude of the FWM signal with coupling detuning and Rabi frequency. It is demonstrated that strong resonances occur in the FWM profile at frequencies symmetrically displaced from the frequency of the coupling field by coupling detuning.

Keywords: electromagnetically induced absorption, coherent hole burning, Mollow absorption, four-wave mixing

PACS: 42.50.Gy, 32.80.QK, 42.65.–K

DOI: 10.1088/1674-1056/ade8e1 **CSTR:** 32038.14.CPB.ade8e1

1. Introduction

Quantum coherences of electromagnetically induced transparency (EIT)[1,2] and electromagnetically induced absorption (EIA)[3–7] have become important techniques for quantum manipulation, simulation, and information processing. Compared with EIT created by destructive interference in the interaction between atoms and lights, EIA with constructive interference has shown an increased sub-natural absorption and has been widely used in atomic clock,[8,9] microwave measurements,[10,11] atomic magnetometry,[12] frequency stability,[13,14] and manipulation of the speed of light pulse.[15–17] The EIA was firstly discovered in degenerate two-level atoms involving multiple Zeeman sublevels coupled with polarized pump beams.[3] It was also investigated in metal–insulator–metal waveguides,[18–22] microresonator systems,[23–26] and one-dimensional photonic crystals.[27] There are typically two types of EIA due to transfer of population (TOP)[28,29] and transfer of coherence (TOC),[29–31] in which the polarizations of the probe and pump beams played a key role and were arranged in parallel or perpendicular. Moreover, considering the complexity of the degenerate two-level system with multiple Zeeman sublevels, the EIA effects in degenerate two-level systems can therefore be simplified as a double two-level scheme corresponding to EIA-TOP[28] and an *N*-type four-level scheme corresponding to EIA-TOC.[32–35] The different mechanisms of TOP and TOC were then revealed due to the collisional induced TOP between ground states[29] and optical pumping induced TOC between excited and ground states.[28]

Mollow absorption (MA)[36,37] is a classical spectral phenomenon and was theoretically predicted by Mollow in 1969[38] and experimentally confirmed in 1974.[39] Coherent hole burning (CHB) is also a classical spectral phenomenon[40] and was first discovered in experiments by Bloembergen *et al.* and theoretically explained by them. Boyd *et al.* theoretically analyzed a two-level atomic system driven by a coupling light and monitored by a probe light, and demonstrated the acquisition of MA under pure spontaneous emission broadening and the acquisition of CHB under rapid collision dephasing.[41] To study the mutual influence of EIT and CHB, Berman *et al.* introduced this two-level model into the Λ-type three-level system and studied the four-wave mixing (FWM) signal spectrum.[42] Gu *et al.* also introduced it into the tripod-type four-level system, which is evolved from the degenerate two-level system subject to a magnetic field. They studied the linear absorption spectrum and explored the application potential in slow light and fast light,[43] and multi-peaked structure of the FWM spectra that was explained as resonant emission between the 'virtual states' in the dressed picture.[44] Goren *et al.* introduced this two-level model into the double TLS of EIA due to TOP, where one TLS corresponds to the sub-natural absorption part of EIA and the other

†Corresponding author. E-mail: yingjied@nwu.edu.cn

© 2025 Chinese Physical Society and IOP Publishing Ltd. All rights, including for text and data mining, AI training, and similar technologies, are reserved.

TLS corresponds to the natural absorption part of EIA. Our recent work has also studied the tripod-type four-level system and discovered the double EIA effect under the joint participation of EIT and CHB.[45]

Although EIA-TOP showed a narrower peak in the presence of Doppler broadening, this kind of EIA peak is still far from that of EIA-TOC in the N-type model, and is often overlooked in experiments.[28,29] It is noted that some interesting results regarding FWM nonlinearity have been demonstrated: the FWM signal spectrum of EIA-TOC is similar to its absorption spectrum, while that of EIA-TOP exhibits characteristics of the EIT absorption spectrum, with the magnitude of its FWM signal constrained. Lezama *et al.* examined FWM in a degenerate two-level system that is driven by a coupling field and probed by a weak field, and found two symmetric sidebands displaced by twice of the generalized Rabi frequency.[46] In this paper, we investigate EIA-TOP and FWM in double TLS. The widths of the sub-natural and natural absorption are determined by spontaneous emission rates of two excited states. The sub-natural absorption part of EIA is governed by CHB while the natural absorption part of EIA is managed by MA. We propose a scheme in which the EIA and FWM can be greatly enhanced through the detuned coupling field.

This paper is organized as follows. In Section 2, we study the model of EIA due to TOP with optical Bloch equations. By inserting the Fourier amplitudes of density matrix elements into the Bloch equations, their Fourier amplitudes including the linear and nonlinear responses are attained. In Section 3, we discuss the enhanced EIA under the detuned pumping field. In Section 4, we discuss the FWM spectra of the enhanced EIA, and show their dependence on the coupling detuning and Rabi frequency. Finally, a summary is given in Section 5.

2. Model and theoretical approach

The EIA-TOP occurs in a degenerate TLS, where the $F_e = F_g + 1$ and $F_g > 0$, which is coupled and probed by fields of the same circular polarization. Figure 1(a) shows a degenerate TLS for transition $F_g = 2 \to F_e = 3$, whose Zeeman sublevels of excited states are $|e_{-3}\rangle$, $|e_{-2}\rangle$, $|e_{-1}\rangle$, $|e_0\rangle$, $|e_1\rangle$, $|e_2\rangle$, and $|e_3\rangle$ for $m_e = -3,-2,-1,0,1,2,3$, and Zeeman sublevels of ground states are $|g_{-2}\rangle$, $|g_{-1}\rangle$, $|g_0\rangle$, $|g_1\rangle$, and $|g_2\rangle$ for $m_g = -2,-1,0,1,2$. The coupling and probe fields with the same circular polarization σ_+ interact with the transitions $m_g = i \to m_e = i+1$ ($i = 0,\pm1,\pm2$), and five TLSs are involved. For the five TLSs, some TLSs play a role in the transfer of population and can be ignored, so the coherent system can be modeled by a double TLS, as shown in Fig. 1(b), where the double TLS have different hyperfine dipole matrix elements and are linked by a spontaneous emission. The states $|2\rangle$ and $|4\rangle$ correspond to two excited states, while the states $|1\rangle$ and $|3\rangle$ correspond to two ground states. The transition between $|4\rangle$ and $|1\rangle$ is forbidden due to selection rules. A coupling field ω_c with the circular polarization σ_+ simultaneously interacts with the transitions $|1\rangle \leftrightarrow |2\rangle$ and $|3\rangle \leftrightarrow |4\rangle$ with the Rabi frequencies V_1 and V_2, respectively, where $V_1 = AV_2$ with A^2 being the branching ratio. A weak probe field ω_p with the same circular polarization as the coupling field probes the transitions $|1\rangle \leftrightarrow |2\rangle$ and $|3\rangle \leftrightarrow |4\rangle$ with the Rabi frequencies V_{p_1} and V_{p_2}, respectively, where $V_{p_1} = AV_{p_2}$. To trace the role of either TLS in the double TLS, we denote the detuning of the coupling field to the TLS $|1\rangle \leftrightarrow |2\rangle$ as Δ_1, which is defined by $\Delta_1 = \omega_1 - \omega_{21}$, and denote the detuning of the coupling field to the TLS $|3\rangle \leftrightarrow |4\rangle$ as Δ_2, which is defined by $\Delta_2 = \omega_2 - \omega_{43}$, where $\omega_1 = \omega_2$ due to from the common coupling field. Generally, since the Zeeman sublevels have $\omega_{21} = \omega_{43}$, the two coupling detunings usually have $\Delta_1 = \Delta_2 = \Delta$. The detuning of the probe field to either of the double TLS is equal and denoted as δ. The two-photon detuning of the probe field to the coupling field is $\delta - \Delta$ or $\omega_p - \omega_c$. The spontaneous decay rates from excited state $|2\rangle$ to ground states $|1\rangle$ and $|3\rangle$ are $A^2\Gamma_2$ and $B^2\Gamma_2$, respectively, where $A^2 + B^2 = 1$ with Γ_2 being the spontaneous emission rate of the excited state $|2\rangle$. The spontaneous decay rate from the excited state $|4\rangle$ to the ground state $|3\rangle$ is denoted as Γ_4. Population transferring due to collisions between the two ground states are γ_{13} and γ_{31}, respectively, while those between two excited states are γ_{24} and γ_{42}, respectively.

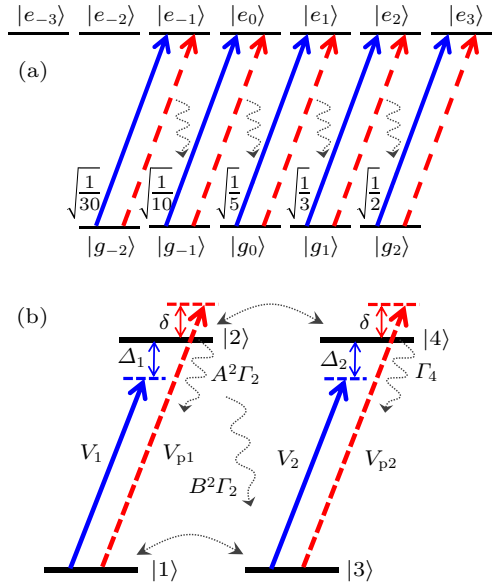


Fig. 1. Schematic energy level diagram of coherent systems of EIA-TOP. Solid lines represent the coupling field and dashed lines are for probe field. (a) The EIA system of a degenerate two-level atomic system ($F_g = 2 \to F_e = 3$) interacts with coupling and probe fields, where the two fields have the same circular polarization σ_+. (b) Simplified EIA model from the degenerate two-level EIA system.

Under dipole and rotating-wave approximation, Bloch equations for the double TLS can be written as

$$\dot{\rho}_{21} = -(i\omega_{21} + \Gamma_2 + \gamma_{13} + \gamma_{24})\rho_{21} - iV_{21}(\rho_{11} - \rho_{22}), \quad (1)$$

$$\dot{\rho}_{43} = -(\mathrm{i}\omega_{43}+\Gamma_4+\gamma_{31}+\gamma_{42})\rho_{43}-\mathrm{i}V_{43}(\rho_{33}-\rho_{44}), \quad (2)$$

$$\dot{\rho}_{11} = -2\gamma_{13}\rho_{11}+2A^2\Gamma_2\rho_{22}+2\gamma_{31}\rho_{33} -\mathrm{i}V_{21}^*\rho_{21}+\mathrm{i}V_{21}\rho_{12}, \quad (3)$$

$$\dot{\rho}_{22} = -2(\Gamma_2+\gamma_{24})\rho_{22}+2\gamma_{42}\rho_{44}-\mathrm{i}V_{21}\rho_{12}+\mathrm{i}V_{21}^*\rho_{21}, \quad (4)$$

$$\dot{\rho}_{33} = 2\gamma_{13}\rho_{11}+2B^2\Gamma_2\rho_{22}-2\gamma_{31}\rho_{33}+2\Gamma_4\rho_{44} +\mathrm{i}V_{43}\rho_{34}-\mathrm{i}V_{43}^*\rho_{43}, \quad (5)$$

$$\dot{\rho}_{44} = -2(\Gamma_4+\gamma_{42})\rho_{44}+2\gamma_{24}\rho_{22}-\mathrm{i}V_{43}\rho_{34}+\mathrm{i}V_{43}^*\rho_{43}. \quad (6)$$

In Eqs. (1)–(6), the density matrix elements are constrained by the relation $\rho_{ij}(\omega_k)=\rho_{ji}^*(-\omega_k)$ and population conservation formula $\rho_{11}+\rho_{22}+\rho_{33}+\rho_{44}=1$. Ignoring the effect of spatial amplitude, the interaction energy for double transitions can be expressed as

$$V_{21} = -\hbar V_1(\omega_1)\exp(-\mathrm{i}\omega_1 t)-\hbar V_{\mathrm{p}_1}(\omega_\mathrm{p})\exp(-\mathrm{i}\omega_\mathrm{p}t), \quad (7)$$

$$V_{43} = -\hbar V_2(\omega_2)\exp(-\mathrm{i}\omega_2 t)-\hbar V_{\mathrm{p}_2}(\omega_\mathrm{p})\exp(-\mathrm{i}\omega_\mathrm{p}t), \quad (8)$$

where $2V_{21}(\omega_1)=\mu_{21}E_{21}(\omega_1)/2^{1/2}\hbar$ and $2V_{43}(\omega_1)=\mu_{43}E_{43}(\omega_1)/2^{1/2}\hbar$ are the Rabi frequencies for the interactions between the coupling field and the atomic transitions $|1\rangle\leftrightarrow|2\rangle$ and $|3\rangle\leftrightarrow|4\rangle$, respectively. While $2V_{\mathrm{p}_1}(\omega_\mathrm{p})=\mu_{21}E_\mathrm{p}(\omega_\mathrm{p})/2^{1/2}\hbar$ and $2V_{\mathrm{p}_2}(\omega_\mathrm{p})=\mu_{43}E_\mathrm{p}(\omega_\mathrm{p})/2^{1/2}\hbar$ are the Rabi frequencies for the interactions between the probe field and the atomic transitions $|1\rangle\leftrightarrow|2\rangle$ and $|3\rangle\leftrightarrow|4\rangle$, respectively. μ_{21} and μ_{43} are hyperfine dipole matrix elements for transitions $|1\rangle\leftrightarrow|2\rangle$ and $|3\rangle\leftrightarrow|4\rangle$, respectively, and have different values in double TLS. If we restore double TLS to the degenerate two-level system as shown in Fig. 1(a), the hyperfine dipole matrix elements are governed by

$$\langle F_\mathrm{g}\, m_\mathrm{g}|er|F_\mathrm{e}\, m_\mathrm{e}\rangle = (-1)^{F_\mathrm{e}-1+m_\mathrm{g}}\langle F_\mathrm{g}||er||F_\mathrm{e}\rangle \times\sqrt{2F_\mathrm{g}+1}\begin{pmatrix} F_\mathrm{e} & 1 & F_\mathrm{g} \\ -m_\mathrm{e} & 1 & m_\mathrm{g}\end{pmatrix}. \quad (9)$$

Notice that in the 3-j symbol, the Zeeman sublevels satisfy $m_\mathrm{e}-m_\mathrm{g}=1$ due to circular polarization σ_+.

In the following Fourier series expansion is to be used. We treat the coupling field to all orders and the probe field to the first order. In the steady state, the elements of the density matrix are expressed as the terms of Fourier amplitudes. For example, the density matrix element ρ_{21} can oscillate at three frequencies: the pump frequency ω_1, the probe frequency ω_p, and the four-wave mixing frequency $2\omega_1-\omega_\mathrm{p}$. So the density matrix elements can be written as

$$\rho_{21} = \rho_{21}(\omega_1)\exp(-\mathrm{i}\omega_1 t)+\rho_{21}(\omega_\mathrm{p})\exp(-\mathrm{i}\omega_\mathrm{p}t) +\rho_{21}(2\omega_1-\omega_\mathrm{p})\exp[-\mathrm{i}(2\omega_1-\omega_\mathrm{p})t], \quad (10)$$

$$\rho_{43} = \rho_{43}(\omega_2)\exp(-\mathrm{i}\omega_2 t)+\rho_{43}(\omega_\mathrm{p})\exp(-\mathrm{i}\omega_\mathrm{p}t) +\rho_{43}(2\omega_2-\omega_\mathrm{p})\exp[-\mathrm{i}(2\omega_2-\omega_\mathrm{p})t], \quad (11)$$

$$\rho_{11(22)} = \rho_{11(22)}^\mathrm{dc}+\rho_{11(22)}(\omega_1-\omega_\mathrm{p})\exp[-\mathrm{i}(\omega_1-\omega_\mathrm{p})t] +\rho_{11(22)}(\omega_\mathrm{p}-\omega_1)\exp[-\mathrm{i}(\omega_\mathrm{p}-\omega_1)t], \quad (12)$$

$$\rho_{33(44)} = \rho_{33(44)}^\mathrm{dc}+\rho_{33(44)}(\omega_2-\omega_\mathrm{p})\exp[-\mathrm{i}(\omega_2-\omega_\mathrm{p})t] +\rho_{33(44)}(\omega_\mathrm{p}-\omega_2)\exp[-\mathrm{i}(\omega_\mathrm{p}-\omega_2)t]. \quad (13)$$

In above equations, the terms $\rho_{21}(\omega_\mathrm{p})$ and $\rho_{43}(\omega_\mathrm{p})$ are related with the absorption spectra for the TLS $|1\rangle\leftrightarrow|2\rangle$ and $|3\rangle\leftrightarrow|4\rangle$, respectively, while the terms $\rho_{21}(2\omega_1-\omega_\mathrm{p})$ and $\rho_{43}(2\omega_2-\omega_\mathrm{p})$ are linked with the FWM spectra of the double TLS, respectively. We insert the interaction energy Eqs. (7) and (8), and Fourier amplitudes of density matrix elements Eqs. (10)–(13) into Eqs. (1)–(6) so that a series of equations for Fourier amplitudes can be obtained. We solve these equations in two stages. In the first stage, the system interacts solely with the coupling field, so the following equations for Fourier amplitudes are involved:

$$\dot{\rho}_{21}^0 = [\mathrm{i}\Delta_1-(\Gamma_2+\gamma_{13}+\gamma_{24})]\rho_{21}(\omega_1)+\mathrm{i}V_1(\rho_{11}^\mathrm{dc}-\rho_{22}^\mathrm{dc}), \quad (14)$$

$$\dot{\rho}_{43}^0 = [\mathrm{i}\Delta_2-(\Gamma_4+\gamma_{31}+\gamma_{42})]\rho_{43}(\omega_2)+\mathrm{i}V_2(\rho_{33}^\mathrm{dc}-\rho_{44}^\mathrm{dc}), \quad (15)$$

$$\dot{\rho}_{11}^0 = \mathrm{i}V_1^*(-\omega_1)\rho_{21}(\omega_1)-\mathrm{i}V_1(\omega_1)\rho_{12}(-\omega_1) +2A^2\Gamma_2\rho_{22}^\mathrm{dc}-2\gamma_{13}\rho_{11}^\mathrm{dc}+2\gamma_{31}\rho_{33}^\mathrm{dc}, \quad (16)$$

$$\dot{\rho}_{22}^0 = \mathrm{i}V_1(\omega_1)\rho_{12}(-\omega_1)-\mathrm{i}V_1^*(-\omega_1)\rho_{21}(\omega_1) -2(\Gamma_2+\gamma_{24})\rho_{22}^\mathrm{dc}+2\gamma_{42}\rho_{44}^\mathrm{dc}, \quad (17)$$

$$\dot{\rho}_{44}^0 = \mathrm{i}V_2(\omega_2)\rho_{34}(-\omega_2)-\mathrm{i}V_2^*(-\omega_2)\rho_{43}(\omega_2) -2(\Gamma_4+\gamma_{42})\rho_{44}^\mathrm{dc}+2\gamma_{24}\rho_{22}^\mathrm{dc}. \quad (18)$$

In a steady state, the time derivatives in Eqs. (14)–(18) are zero. The above linear equations can be solved based on the closed condition. In the second stage, the probe field is included to the first order. We can further write out the equations about Fourier amplitudes as follows:

$$\dot{\rho}_{21}(\omega_\mathrm{p}) = [\mathrm{i}\delta-(\Gamma_2+\gamma_{13}+\gamma_{24})]\rho_{21}(\omega_\mathrm{p})+\mathrm{i}V_{\mathrm{p}_1}(\omega_\mathrm{p})(\rho_{11}^\mathrm{dc}-\rho_{22}^\mathrm{dc})+\mathrm{i}V_1(\omega_1)[\rho_{11}(\omega_\mathrm{p}-\omega_1)-\rho_{22}(\omega_\mathrm{p}-\omega_1)], \quad (19)$$

$$\dot{\rho}_{21}(2\omega_1-\omega_\mathrm{p}) = [\mathrm{i}(-\delta+2\Delta_1)-(\Gamma_2+\gamma_{13}+\gamma_{24})]\rho_{21}(2\omega_1-\omega_\mathrm{p})+\mathrm{i}V_1(\omega_1)[\rho_{11}(\omega_1-\omega_\mathrm{p})-\rho_{22}(\omega_1-\omega_\mathrm{p})], \quad (20)$$

$$\dot{\rho}_{43}(\omega_\mathrm{p}) = [\mathrm{i}\delta-(\Gamma_4+\gamma_{31}+\gamma_{42})]\rho_{43}(\omega_\mathrm{p})+\mathrm{i}V_{\mathrm{p}_2}(\omega_\mathrm{p})(\rho_{33}^\mathrm{dc}-\rho_{44}^\mathrm{dc})+\mathrm{i}V_2(\omega_2)[\rho_{33}(\omega_\mathrm{p}-\omega_2)-\rho_{44}(\omega_\mathrm{p}-\omega_2)], \quad (21)$$

$$\dot{\rho}_{43}(2\omega_2-\omega_\mathrm{p}) = [\mathrm{i}(-\delta+2\Delta_2)-(\Gamma_4+\gamma_{31}+\gamma_{42})]\rho_{43}(2\omega_2-\omega_\mathrm{p})+\mathrm{i}V_2(\omega_2)[\rho_{33}(\omega_2-\omega_\mathrm{p})-\rho_{44}(\omega_2-\omega_\mathrm{p})], \quad (22)$$

$$\dot{\rho}_{11}(\omega_1-\omega_\mathrm{p}) = [\mathrm{i}(\Delta_1-\delta)-2\gamma_{13}]\rho_{11}(\omega_1-\omega_\mathrm{p})+\mathrm{i}V_1^*(-\omega_1)\rho_{21}(2\omega_1-\omega_\mathrm{p})+\mathrm{i}V_{\mathrm{p}_1}^*(-\omega_\mathrm{p})\rho_{21}(\omega_1) -\mathrm{i}V_1(\omega_1)\rho_{12}(-\omega_\mathrm{p})+2A^2\Gamma_2\rho_{22}(\omega_1-\omega_\mathrm{p})+2\gamma_{31}\rho_{33}(\omega_1-\omega_\mathrm{p}), \quad (23)$$

$$\dot{\rho}_{22}(\omega_1-\omega_\mathrm{p}) = [\mathrm{i}(\Delta_1-\delta)-2(\Gamma_2+\gamma_{24})]\rho_{22}(\omega_1-\omega_\mathrm{p})-\mathrm{i}V_1^*(-\omega_1)\rho_{21}(2\omega_1-\omega_\mathrm{p})-\mathrm{i}V_{\mathrm{p}_1}^*(-\omega_\mathrm{p})\rho_{21}(\omega_1)$$

$$+\mathrm{i}V_1(\omega_1)\rho_{12}(-\omega_\mathrm{p})+2\gamma_{42}\rho_{44}(\omega_1-\omega_\mathrm{p}), \tag{24}$$

$$\dot{\rho}_{44}(\omega_2-\omega_\mathrm{p}) = [\mathrm{i}(\Delta_2-\delta)-2(\Gamma_4+\gamma_{42})]\rho_{44}(\omega_2-\omega_\mathrm{p})-\mathrm{i}V_2^*(-\omega_2)\rho_{43}(2\omega_2-\omega_\mathrm{p})-\mathrm{i}V_{\mathrm{p}_2}^*(-\omega_\mathrm{p})\rho_{43}(\omega_2)$$
$$+\mathrm{i}V_2(\omega_2)\rho_{34}(-\omega_\mathrm{p})+2\gamma_{24}\rho_{22}(\omega_2-\omega_\mathrm{p}). \tag{25}$$

The constant terms in the above equations are provided by the solution of the equations without the probe field.

The probe absorption spectra and refractions are proportional to the imaginary and real parts of the susceptibility $\chi(\omega_\mathrm{p})\propto[\mu_{21}\rho_{21}(\omega_\mathrm{p})/V_{\mathrm{p}_1}+\mu_{43}\rho_{43}(\omega_\mathrm{p})/V_{\mathrm{p}_2}]$, where $\mu_{21}=A\mu_{43}$, $V_1=AV_2$ and $V_{\mathrm{p}_1}=AV_{\mathrm{p}_2}$. The probe Rabi frequency is very small and in this paper is always fixed in $V_{\mathrm{p}_2}=0.01\Gamma_4$. A value of $A=0.816$ is used, which corresponds to σ_+ transitions of the $F_\mathrm{g}=2\rightarrow F_\mathrm{e}=3$ cycling transition in ^{87}Rb.[28] In addition, atomic decay rates, detunings of the optical field and Rabi frequencies are expressed by the spontaneous emission rate Γ_4. In the double TLS, the relaxation rates between two ground states γ_{13} and γ_{31} are different from those between two excited states γ_{24} and γ_{42}.

3. Enhanced EIA by detuned coupling field

Figure 2 illustrates the enhanced EIA in the presence of a detuned coupling field where $\Delta=\Delta_1=\Delta_2$. In the case where the coupling detuning is zero, it can be seen that the EIA effect is quite weak. From the inset image, it can be seen that at the top of the absorption peak is a small dip, which is the manifestation of the CHB effect. However, as the coupling field is detuned to $\Delta=0.5\Gamma_4$, the sub-natural absorption increases significantly. It can be seen that the magnitude of the sub-natural absorption part of the EIA enhances by at least one order of magnitude compared to the case when the coupling detuning is zero, and reaches 80% that of the natural absorption part of the EIA (where the magnitude of the natural absorption part keeps roughly fixed in the varying coupling detunings because of the fixed population in the state $|3\rangle$, which can be interpreted in Fig. 7), in sharp contrast to only 2% the magnitude of the natural absorption part when the coupling detuning is zero. As $\Delta=2\Gamma_4$, the magnitude of sub-natural absorption is 67% that of natural absorption, still in sharp contrast to the case without detuning. However, with the increase of coupling detuning, the magnitude of sub-natural absorption has a slowdown. We find that when coupling detuning $\Delta=9\Gamma_4$ which cannot be shown in Fig. 2, the magnitude of the sub-natural absorption part reduces to 66% that of the natural absorption part, still about 30 times that when coupling detuning is zero.

We attribute the enhancement of EIA to the fact that the pumping efficiency of the coupling field drops with the detuned coupling field. In this double TLS, populations are pumped to states $|3\rangle$ and $|4\rangle$ from states $|1\rangle$ and $|2\rangle$ under coupling field. As the coupling field is detuned, the pumping becomes weakened, resulting in a rapid reflux of the population at the state $|1\rangle$. Since TLS $|1\rangle\leftrightarrow|2\rangle$ is responsible for the sub-natural absorption part of the EIA (this will be shown in Fig. 4), the rise of population at state $|1\rangle$ leads to the growth of the sub-natural absorption part of the EIA. In addition, we notice that although there is a certain coupling detuning, the absorption spectra of EIA maintain good symmetry, and we attribute it to the equal frequency shift of the sub-natural and natural absorptions of EIA. We also notice that the enhanced EIA appears at the position of $-\Delta$, opposite to the sign of the coupling detuning. The cause for this phenomenon is the definition of the two-photon detuning $\delta-\Delta$, where the negative sign before the term Δ makes the enhanced EIA occur in the negative two-photon detuning.

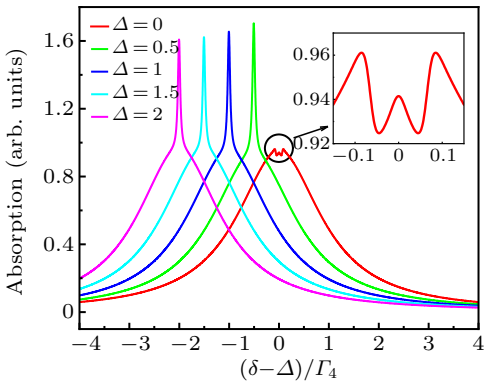


Fig. 2. Probe absorption spectra for different coupling detunings where $\Delta=\Delta_1=\Delta_2$ at $V_2=0.1\Gamma_4$, $A=0.816$, $V_{\mathrm{p}_2}=0.01\Gamma_4$, $\gamma_{24}=\gamma_{42}=0.01\Gamma_4$, $\Gamma_2=0.05\Gamma_4$, $\gamma_{13}=0.005\Gamma_4$, and $\gamma_{31}=0.0001\Gamma_4$. The sub-natural absorption of EIA is greatly increased under the detuned coupling field.

Figure 3 illustrates the impact of the parameter A on the EIA. It is clear that the EIA effect is enhanced with the increase of the parameter A, in which sub-natural absorption assumes nearly all the enhancement while natural absorption does not. In terms of refraction, according to the Kramers–Kronig relation, the magnitude of the refractive index enhances with the increase of the parameter A. Besides, the sub-natural absorption part corresponds to a steep anomalous dispersion while the natural absorption part corresponds to an anomalous dispersion. This steep dispersion is useful in superluminal and even negative group velocities. Although different A are shown in this discussion, they are actually related to the hyperfine dipole matrix elements of Zeeman sublevel transitions, shown in Eq. (9). In the circular transition of ^{87}Rb the parameter A is not only related to the total angular momenta of the excited state and the ground state, but also related to the polarization of the applied optical field. In the D_2 line $F_\mathrm{g}=2\rightarrow F_\mathrm{e}=3$, the parameter A reaches 0.816 for the σ_+

transition. While in the D_2 line $F_g = 1 \to F_e = 2$, it becomes $A = 0.707$ for the same circular polarization. Thus, at least two different values of A can be obtained in the same atomic medium. In the experiment, based on the D_2 line of the ^{87}Rb atom, we can use the same right-handed circularly polarized field for the orbital angular momenta $F_g = 1 \to F_e = 2$ and $F_g = 2 \to F_e = 3$ to obtain $A = 0.707$ and $A = 0.816$, respectively.

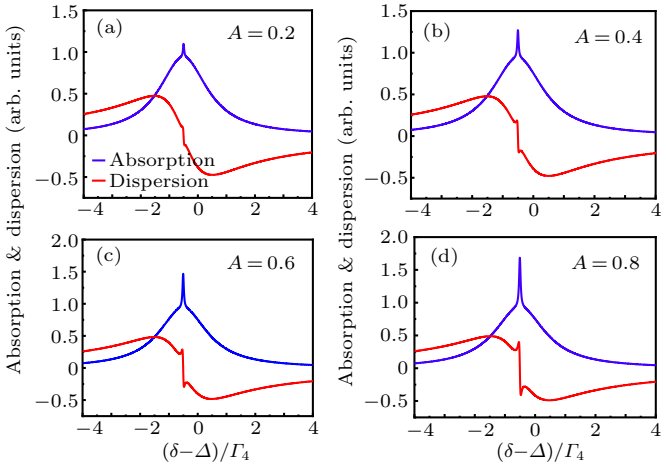


Fig. 3. The absorption and dispersion of EIA at coupling detuning $\Delta = 0.5\Gamma_4$ with $\Delta = \Delta_1 = \Delta_2$ for different A. The other parameters are the same as those in Fig. 2. The sub-natural absorption of EIA enhances with the increase of A.

Now we discuss the individual behavior of either probe absorption spectrum. We consider that the coupling field has different detunings from the double TLS and define the detuning of the coupling field from the TLS $|1\rangle \leftrightarrow |2\rangle$ as Δ_1, and the detuning of the coupling field from the TLS $|3\rangle \leftrightarrow |4\rangle$ as Δ_2. If detuning $\Delta_2 = 0$ and letting detuning Δ_1 vary, the role of coupling field in TLS $|1\rangle \leftrightarrow |2\rangle$ can be found. Figure 4(a) illustrates the absorption spectra of EIA in different detunings Δ_1 with $\Delta_2 = 0$. It is seen that the natural absorption remains fixed, while the sub-natural absorption moves with the detuning Δ_1. So we can deduce that the coupling field in TLS $|1\rangle \leftrightarrow |2\rangle$ governs the sub-natural absorption part of the EIA. It can be further verified by Fig. 4(b), in which the absorption spectrum of the probe field V_{p_1} corresponds to a pure sub-natural absorption, and the absorption spectrum of the probe field V_{p_2} corresponds to a natural absorption. Thus, TLS $|1\rangle \leftrightarrow |2\rangle$ and $|3\rangle \leftrightarrow |4\rangle$ are responsible for the sub-natural and natural absorption parts of EIA, respectively. The widths of the sub-natural and natural absorption are determined by spontaneous emission rates Γ_2 and Γ_4, respectively.

Next, we examine the impact of coupling Rabi frequency on EIA. In Fig. 5, we plot the absorption spectra of EIAs in different coupling Rabi frequencies at $\Delta = 0.5\Gamma_4$. It is clear that with the increase of the coupling Rabi frequency, the sub-natural absorption of the EIA becomes broadened and fades away gradually, and the magnitude of the absorption spectra decreases significantly, while the absorption spectra of the EIA lose symmetry. The natural absorption of EIA is governed by the detuned MA, while the sub-natural absorption of EIA is governed by the detuned CHB. It can be seen that when the coupling Rabi frequency increases to $V_2 = 0.7\Gamma_4$, the magnitude of the absorption spectrum is 0.63 which only 37% that of absorption when $V_2 = 0.1\Gamma_4$, and the sub-natural absorption part of the EIA is gone. The EIA due to TOC also degrades with the increase of the coupling Rabi frequency and turns into an absorption spectrum with four peaks.[28] Therefore, large coupling Rabi frequencies should be avoided for the presence of EIA.

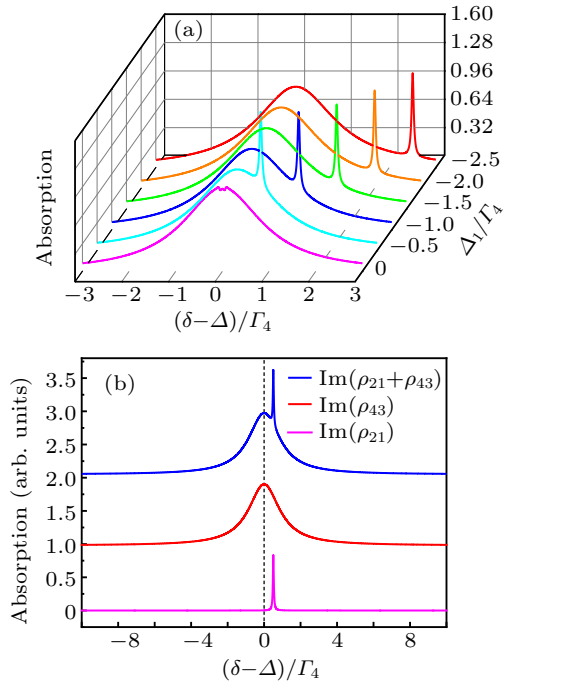


Fig. 4. (a) Probe absorption spectra with $\Delta_2 = 0$ and different coupling detunings Δ_1, (b) probe absorption spectra with $\Delta_1 = -0.5\Gamma_4$ and $\Delta_2 = 0$ for TLS $|1\rangle \leftrightarrow |2\rangle$, $|3\rangle \leftrightarrow |4\rangle$ and double TLS, respectively. The other parameters are the same as those in Fig. 2. TLS $|1\rangle \leftrightarrow |2\rangle$ is responsible for the sub-natural absorption part of EIA, and TLS $|3\rangle \leftrightarrow |4\rangle$ for the natural absorption part of EIA.

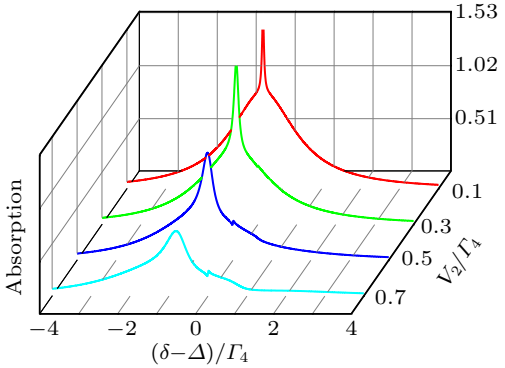


Fig. 5. Probe absorption spectra in different coupling Rabi frequencies at $\Delta_1 = \Delta_2 = 0.5\Gamma_4$. The other parameters are the same as those in Fig. 2. EIA decreases and loses symmetry with the increase of the coupling Rabi frequency.

Another area of interest is the impact of the transit time of the optical field in the thermal atoms on the EIA. In this system, the relaxation rates from atomic collisions have the same

function as decay due to the transit time. γ_{31} and γ_{13} are the relaxation rates between the two ground states and γ_{42} and γ_{24} are the relaxation rates between the two excited states. The values of the relaxation rates γ_{42} and γ_{24} are generally different from those of the relaxation rates γ_{31} and γ_{13} because of the unbalanced states. The function of the relaxation rate γ_{13} is to transfer populations from the state $|1\rangle$ to $|3\rangle$, while γ_{31} is just the opposite. Figure 6 shows the absorption and dispersion of the EIA at different relaxation rates γ_{31}. It can be seen that the magnitude of the sub-natural absorption part of the EIA enhances with the increase of the relaxation rate γ_{31}, while that of the natural absorption remains almost unchanged. This process is closely related to the population of the state $|1\rangle$. With the increase of γ_{31} the population of state $|1\rangle$ undergoes an increase as well. The increase of population directly leads to the growth of the sub-natural absorption part of the EIA. In the following, the influence of the variation in populations on EIA will be specifically described.

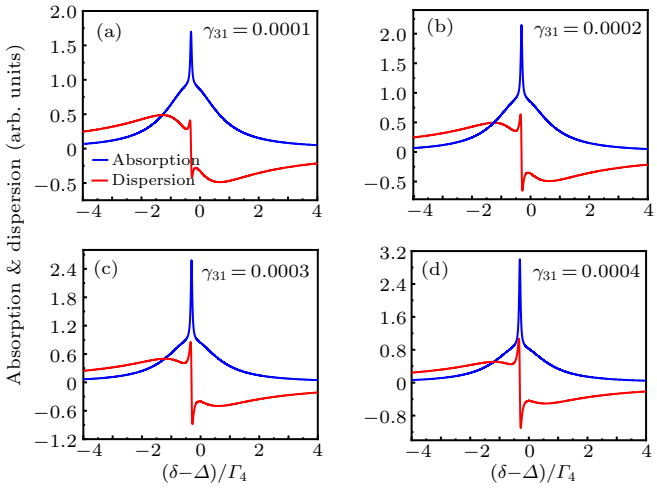


Fig. 6. Absorption and dispersion of EIA with collisional decay rates $\gamma_{42} = \gamma_{24} = 0.01\Gamma_4$, $\gamma_{13} = 0.005\Gamma_4$ and different γ_{31}. The other parameters are the same as those in Fig. 2. EIA is significantly enhanced with the increase of the collisional decay rate γ_{31}.

The detuned coupling field leads to an enhanced EIA. We now examine the impact of coupling detuning on populations in four states of the system. Figure 7 shows the populations of the four states as functions of coupling detuning. As $\Delta = 0$, atoms are pumped to state $|3\rangle$ because of the pumping effect of the coupling field. It can be seen that there are $\rho_{11} = 0.0016$, $\rho_{22} = 5.4 \times 10^{-4}$ and $\rho_{44} = 0.0096$, while the population ρ_{33} reaches 0.9883, which is much larger than those at states $|1\rangle$, $|2\rangle$ and $|4\rangle$. However, as the coupling field is detuned, the population ρ_{11} has a rapid rise, reaching the maximum 0.0290 at $\Delta = 0.38\Gamma_4$, and then has a slowdown. However, the population at state $|3\rangle$ exhibits a contrary evolution. Initially, it undergoes a rapid decline until it reaches its minimum 0.9630, and then has a gradual growth. The population at state $|2\rangle$ or $|4\rangle$ has a monotonic decrease due to the three-photon effect (as shown in Fig. 8(b)). The magnitude of the natural absorption part of the EIA is nearly unchanged because there are only small changes in the population at state $|3\rangle$. However, the population at state $|1\rangle$ is closely related to the enhanced sub-natural absorption part of the EIA because the more atoms at state $|1\rangle$ the more probe field will be absorbed to reach state $|2\rangle$. With the further increase of coupling detuning, the rise of the population is replaced by a slowdown which also makes the magnitude of the sub-natural absorption part have a slowdown. We attribute slowdown of the population at state $|1\rangle$ to the role of the three-photon effect, which strengthens the pumping efficiency of the coupling field.

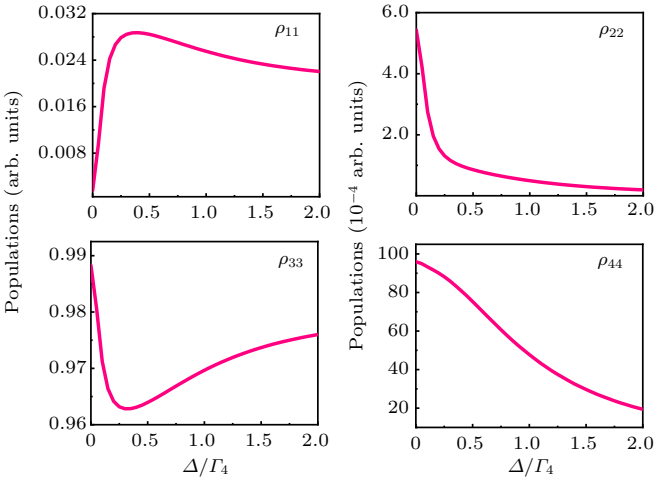


Fig. 7. Populations of double TLS as functions of coupling detuning. The other parameters are the same as those in Fig. 2. The population ρ_{11} has an enormous increase in the initial increase of coupling detuning, which leads to enhanced absorption of EIA.

4. FWM signal spectra for enhanced EIA

The probe FWM spectra are described by the terms $\rho_{21}(2\omega_1 - \omega_p)$ and $\rho_{43}(2\omega_2 - \omega_p)$, respectively. They correspond to two FWMs and the overall FWM is the sum of these two FWMs. Figure 8(a) exhibits the FWM spectra of the enhanced EIA in parameters $V_2 = 0.3\Gamma_4$, $\Delta = 0.5\Gamma_4$ and other parameters are the same as those in Fig. 2. In Fig. 8(a), we let FWM_1 and FWM_2 represent $|\rho_{21}(2\omega_1 - \omega_p)|$ and $|\rho_{43}(2\omega_2 - \omega_p)|$, respectively, and let FWM denote $|\rho_{21}(2\omega_1 - \omega_p)|+|\rho_{43}(2\omega_2 - \omega_p)|$. It can be seen from the figure that FWM_1 shows three sharp peaks, while FWM_2 shows a peak with Lorentzian distribution. The FWM signal at $\delta - \Delta = 0$ corresponds to a degenerate FWM. It is noted that the sub-natural absorption part of the EIA corresponds to two symmetric sidebands in the FWM_1 spectrum due to the effect of CHB. To interpret the phenomenon, we plot a model of states, as shown in Fig. 8(b). At low coupling Rabi frequency, the detuned coupling field induces two virtual states, which are located above the ground state and below the excited state as the coupling detuning $\Delta < 0$, or which are located below the ground state and above the excited state as the coupling detuning $\Delta > 0$, with a frequency shift of $|\Delta|$ from the solid state. The energy level diagram corresponds to the case where the coupling detuning $\Delta < 0$. It can be seen that

the energy difference between the ground virtual state and the ground state $|1\rangle$ is $-\hbar\Delta$, while the energy difference between the excited virtual state and the excited state $|2\rangle$ is also $-\hbar\Delta$. The probe field with frequency $\omega_p = \omega_c$ ($\delta = \Delta$), drives population of the ground state to the excited virtual state. Subsequently, due to the instability of the virtual state, a photon with frequency $\omega_p + \Delta$ is radiated to the ground virtual state. Then the probe field with frequency $\omega_p = \omega_c$, drives population of the ground virtual state to the excited state. Finally, a photon with frequency $\omega_p - \Delta$ is radiated to the ground state. In the process of three-photon effect two FWM signals in frequency $\omega_p \pm \Delta$ is generated, corresponding to two FWM sidebands. It is noted that at large coupling Rabi frequencies, the distance between the two sidebands becomes twice the generalized Rabi frequency. Symmetrical sidebands of the FWM signal were also found in the degenerate two-level system.[46]

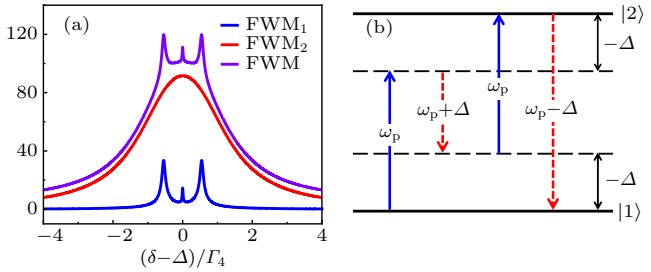


Fig. 8. (a) FWM spectra of TLS $|1\rangle \leftrightarrow |2\rangle$, $|3\rangle \leftrightarrow |4\rangle$, and double TLS in parameters $V_2 = 0.3\Gamma_4$, $\Delta = 0.5\Gamma_4$, $A = 0.618$. The other parameters are the same as those in Fig. 2. (b) Schematic diagram of the three-photon effect for TLS $|1\rangle \leftrightarrow |2\rangle$ where $\Delta < 0$. The two sidebands are displaced from the coupling frequency by coupling detuning.

Next, we examine the impact of coupling detuning on the FWM spectra. In Figs. 9(a)–9(c), we plot the FWM spectra in parameters $V_2 = 0.1\Gamma_4$ and $A = 0.816$. It is clear that the increase in coupling detuning leads to modification not only in the magnitude of the FWM signal, but also in the distribution of the FWM spectrum. It can be observed that when $\Delta = 0.1\Gamma_4$ (where $\Delta = \Delta_1 = \Delta_2$), the magnitude of FWM_1 exceeds that of FWM_2 by a factor of 3.5. At a detuning of $\Delta = 0.4\Gamma_4$, however, the magnitude of FWM has a significant reduction, where the magnitude of FWM_1 has only 57% that of FWM_2. And at $\Delta = 0.7\Gamma_4$, the magnitude of FWM_1 is only 36% that of FWM_2. On the other hand, the frequency distance in the sidebands increases with the rise of coupling detuning, and thus changes the distribution of the FWM spectrum. In the above three scenarios, it appears that the increase in coupling detuning leads to a decrease in FWM magnitude. To examine the evolution of FWM with coupling detuning, we plot Fig. 9(d). It illustrates that the magnitudes of the FWM spectra with the increasing coupling detuning initially have a rapid increase, and then a slowdown with their maximums between $\Delta = 0$–$0.5\Gamma_4$. Due to the fact that the magnitude of the FWM is governed by the quantum interference of CHB and MA, a large coupling Rabi frequency is not necessarily detrimental to a large FWM magnitude.

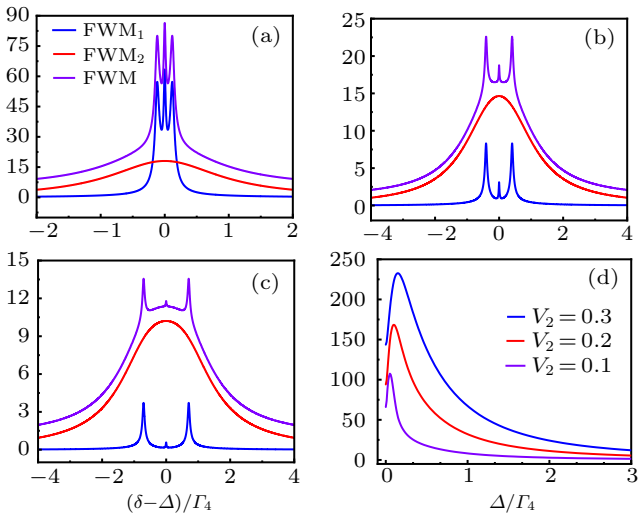


Fig. 9. FWM spectra for TLS $|1\rangle \leftrightarrow |2\rangle$, $|3\rangle \leftrightarrow |4\rangle$ and double TLS in the coupling detunings (a) $\Delta = 0.1\Gamma_4$, (b) $\Delta = 0.4\Gamma_4$ and (c) $\Delta = 0.7\Gamma_4$. The other parameters are the same as those in Fig. 2. (d) The magnitude of the FWM signal as a function of coupling detuning in different coupling Rabi frequencies.

Because the sub-natural and natural absorption parts of EIA are governed by the effects of CHB and MA, respectively, the magnitude of the FWM signal is related to the effects of CHB and MA, even when the EIA vanishes in the absorption spectrum. In Figs. 10(a)–10(c), we plot the FWM spectra in different coupling Rabi frequencies with the parameters $\Delta = 0.3\Gamma_4$ and $A = 0.816$. When $V_2 = 0.1\Gamma_4$, the FWM magnitude is 28, as shown in Fig. 10(a). Further, when $V_2 = 0.4\Gamma_4$, the FWM magnitude reaches 265, which then rises to 340 when $V_2 = 0.7\Gamma_4$, as shown in Figs. 10(b) and 10(c). In the above three scenarios, it appears that the increase in coupling Rabi frequency leads to an increase in FWM magnitude. To examine the evolution of FWM with the coupling Rabi frequency, we plot Fig. 10(d). It illustrates that the FWM magnitude initially has a rise and then a slowdown. It is clear that the growth in Figs. 10(a)–10(c) is a localized event. The above three cases happen precisely during the period of increase. As the coupling Rabi frequency grows further, the CHB and MA are replaced by Autler–Townes (A-T) splitting, and then the FWM becomes small. By comparing the three evolution curves, it can be observed that for a small coupling Rabi frequency, a large coupling detuning is associated with a small FWM response, while for a large coupling Rabi frequency, a large coupling detuning is associated with a large FWM response.

To obtain a more complete picture of the impact of coupling detuning and Rabi frequency on the FWM signal, we plot the magnitude of the FWM spectra as a function of coupling detuning and Rabi frequency in Fig. 11. This global map includes the magnitudes of the FWM signals with coupling detuning in Fig. 9(d), and the magnitudes of the FWM signals with the coupling Rabi frequency in Fig. 10(d). The figure shows that the detuned coupling field and the increase in the coupling Rabi frequency can bring enhancements to FWM. It

is worth noting that a strong coupling field can cause the EIA to disappear due to the reduction of the magnitude and the broadening of the absorption spectrum, but in terms of the response of the FWM nonlinearity, it is not synchronous with the enhancement of EIA, because the magnitude of the FWM signal is governed by the the coherent effects of CHB and MA. It can be seen that when there is a large coupling detuning but no large coupling Rabi frequency, the FWM signal will still be very small, so an appropriate coupling Rabi frequency combined with an appropriate coupling detuning can bring a large magnitude of FWM. With the further increase of the coupling Rabi frequency, however, the coherent effects of CHB and MA will be replaced by A-T splitting, and in this case the quantum interference of CHB and MA and the enhanced FWM nonlinearity will completely disappear. This result is also consistent with literature in which the magnitude of the FWM signal first increases and then decreases with the increasing Rabi frequency of the coupling field.[46]

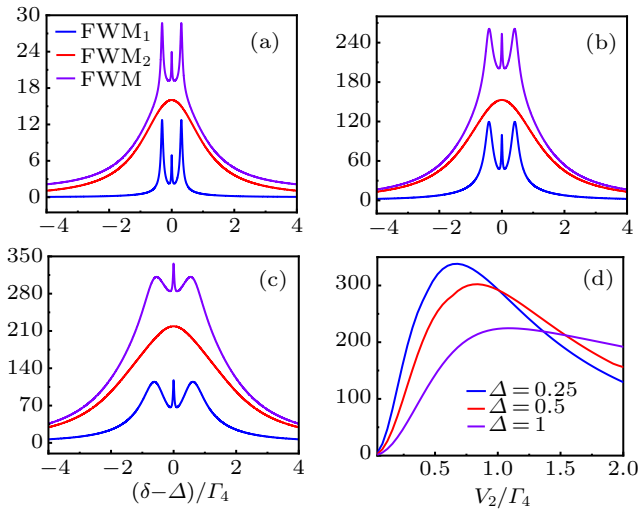


Fig. 10. FWM spectra for TLS $|1\rangle \leftrightarrow |2\rangle$, $|3\rangle \leftrightarrow |4\rangle$ and double TLS in the coupling Rabi frequencies (a) $V_2 = 0.1\Gamma_4$, (b) $V_2 = 0.4\Gamma_4$ and (c) $V_2 = 0.7\Gamma_4$. The other parameters are the same as those in Fig. 2. (d) The magnitude of the FWM signal as a function of coupling Rabi frequency in different coupling detunings.

In addition to the coupling detuning and Rabi frequency that have an obvious influence on the magnitude of the FWM, there are other parameters that have a significant effect on the FWM. The first parameter is the parameter A that decides the branching ratio of spontaneous emission rate. As the parameter A is very small, the magnitude of the FWM signal is also very small. When A increases near the maximal value of 1, the magnitude of FWM will be significantly enhanced. The second parameters are the relaxation rates between ground states. The relaxation rate γ_{13} plays a role of increasing the population ρ_{33} and reducing the population ρ_{11}, so it is unfavorable to the enhancement of EIA. On the contrary, the relaxation rate γ_{31} plays a role of increasing the population ρ_{11} and reducing the population ρ_{33}, so it is favorable to the enhancement of EIA and FWM. This paper does not consider the impact of the Doppler effect on EIA. In fact, at room temperature, the Doppler effect has a devastating impact on EIA, so we suggest that the experiment should be carried out in the medium of cold atoms.

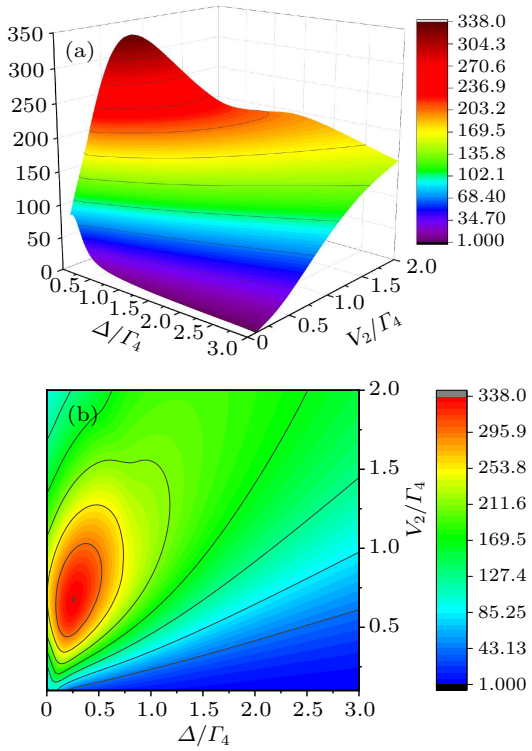


Fig. 11. (a) 3D image and (b) contour map of the magnitude of the FWM versus the detuning and Rabi frequency of the coupling field. The other parameters are the same as those in Fig. 2.

5. Conclusion

We have theoretically explored EIA due to TOP and FWM response in double TLS, where each TLS is simultaneously driven by the coupling and probe fields. Due to the difference in spontaneous emission and population, the CHB effect occurs in TLS $|1\rangle \leftrightarrow |2\rangle$, which is responsible for the sub-natural absorption part of EIA, and the MA effect occurs in the other TLS $|3\rangle \leftrightarrow |4\rangle$, which is responsible for the natural absorption part of EIA. Due to the pumping effect of the coupling field, the vast majority of atoms are pumped into the state $|3\rangle$. Therefore, the detuning of coupling field will reduce the pumping efficiency of the coupling field and thus restore the atomic population to state $|1\rangle$. It was found that when the coupling field is detuned the sub-natural absorption part of the EIA has a rise by two orders of magnitude. In addition to the detuned coupling field that can change the population at the state $|1\rangle$, the relaxation rates between states $|1\rangle$ and $|3\rangle$ also have a crucial influence on the population at state $|1\rangle$. The relaxation rate γ_{13} will reduce the population on state $|1\rangle$, while the relaxation rate γ_{31} is the opposite. Therefore, an increased γ_{13} will reduce EIA, while an increased γ_{31} will increase EIA. It was found that there is a significant enhancement of EIA with a small increase in the relaxation rate γ_{31}. In addition,

we explored the FWM of the enhanced EIA. It was found that the sub-natural absorption of EIA corresponds to the two sidebands of FWM, which are related to the three-photon process, while the natural absorption part of EIA does not. We have explored the magnitude of the FWM signal with coupling detuning and Rabi frequency. Studies have shown that the magnitude of the FWM first increases and then decreases with the increase of detuning and Rabi frequency of the coupling field. This theoretical work may provide a reference for experimental research.

Acknowledgement

Project supported by the Open Subject of the State Key Laboratory of Quantum Optics Technologies and Devices (Grant No. KF202209).

References

[1] Harris S E, Yin G Y, Kasapi A, Jain M and Luo Z F 1996 *Phys. Today* **50** 36
[2] Braje D A, Balić V, Yin G Y and Harris S E 2003 *Phys. Rev. A* **68** 041801
[3] Akulshin A M, Barreiro S and Lezama A 1998 *Phys. Rev. A* **57** 2996
[4] Lezama A, Barreiro S and Akulshin A M 1999 *Phys. Rev. A* **59** 4732
[5] Lipsich A, Barreiro S, Akulshin A M and Lezama A 2000 *Phys. Rev. A* **61** 053803
[6] Renzoni F, Cartaleva S, Alzetta G and Arimondo E 2001 *Phys. Rev. A* **63** 065401
[7] Wu Y Y, He Y H, Jiao Y C and Zhao J M 2024 *Chin. Phys. B* **33** 113201
[8] Vanier J 2005 *Appl. Phys. B* **81** 421
[9] Brazhnikov D, Ignatovich S, Vishnyakov V, Boudot R and Skvortsov M 2019 *Opt. Express* **27** 036034
[10] Thaicharoen N, Moore K R, Anderson D A, Powel R C, Peterson E and Raithel G 2019 *Phys. Rev. A* **100** 063427
[11] You S H, Cai M H, Zhang S S, Xu Z S and Liu H P 2022 *Opt. Express* **30** 16619
[12] Budker D and Romalis M 2007 *Nat. Phys.* **3** 227
[13] Zhao Y T, Zhao J M, Huang T, Xiao L T and Jia S T 2004 *J. Phys. D: Appl. Phys.* **37** 1316
[14] Becerra F E, Willis R T, Rolston S L and Orozco L A 2009 *J. Opt. Soc. Am. B* **26** 1315
[15] Hau L V, Harris S E, Dutton Z and Behroozi C H 1999 *Nature* **397** 594
[16] Bae I H and Moon H S 2011 *Phys. Rev. A* **83** 053806
[17] Naweed A 2021 *OSA Continuum* **4** 2771
[18] Li H J, Zhai X and Wang L L 2015 *Appl. Phys. Express* **8** 092201
[19] Li H J, Wang L L and Zhai X 2016 *IEEE Photon. Technol. Lett.* **28** 1454
[20] Wen K H, Hu Y H, Chen L, Zhou J Y, He M, Lei L and Meng Z M 2016 *IEEE Photon. J.* **8** 1
[21] Liu D D, Pan Y W, Sun Y, Xia X S, Wang J C and Lu J 2016 *AIP Adv.* **6** 025219
[22] Wen K H, Hu Y H, Zhou J Y, Lei L, Li J F and Wu Y J 2017 *Opt. Mater. Express* **7** 433
[23] Bui K V and Rosenberger A T 2020 *Phys. Rev. A* **101** 033836
[24] Bui K V and Rosenberger A T 2022 *Phys. Rev. A* **106** 033504
[25] Naweed A, Farca G, Shopova S I and Rosenberger A T 2005 *Phys. Rev. A* **71** 043804
[26] Wang C Q, Jiang X F, Zhao G M, Zhang M Z, Hsu C W, Peng B, Stone A D, Jiang L and Yang L 2020 *Nat. Phys.* **16** 334
[27] Naweed A 2021 *OSA Continuum* **4** 1358
[28] Goren C, Wilson-Gordon A D, Rosenbluh M and Friedmann H 2004 *Phys. Rev. A* **70** 043814
[29] Goren C, Wilson-Gordon A D, Rosenbluh M and Friedmann H 2003 *Phys. Rev. A* **67** 033807
[30] Failache H, Valente P, Ban G, Lorent V and Lezama A 2003 *Phys. Rev. A* **67** 043810
[31] Zigdon T, Wilson-Gordon A D and Friedmann H 2008 *Phys. Rev. A* **77** 033836
[32] Goren C, Wilson-Gordon A D, Rosenbluh M and Friedmann H 2004 *Phys. Rev. A* **69** 053818
[33] Taichenachev A V, Tumaikin A M and Yudin V I 1999 *Phys. Rev. A* **61** 011802
[34] Pandey K 2013 *Phys. Rev. A* **87** 043838
[35] Dimitrijević J, Arsenović D and Jelenković B M 2007 *Phys. Rev. A* **76** 013836
[36] Mollow B R 1972 *Phys. Rev. A* **5** 2217
[37] Wu F Y, Ezekiel S, Ducloy M and Mollow B R 1977 *Phys. Rev. Lett.* **38** 1077
[38] Mollow B R 1969 *Phys. Rev.* **188** 1969
[39] Schuda F, Jr C R S and Hercher M 1974 *J. Phys. B: Atom. Mol. Phys.* **7** 7
[40] Sharp R C, Yablonovitch E and Bloembergen N 1981 *J. Chem. Phys.* **74** 5357
[41] Boyd R W, Raymer M G, Narum P and Harter D J 1981 *Phys. Rev. A* **24** 411
[42] Berman P R and Xu X D 2008 *Phys. Rev. A* **78** 053407
[43] Gu Y, Sun Q Q and Gong Q H 2004 *Phys. Rev. A* **69** 063805
[44] Sun Q Q, Gu Y and Gong Q H 2006 *J. Mod. Opt.* **53** 1663
[45] Han J Y, Sun Y and Du Y J 2025 *Appl. Phys. B* **131** 8
[46] Lezama A, Cardoso G C and Tabosa J W R 2000 *Phys. Rev. A* **63** 013805